Progress of Theoretical Physics, Vol. 95, No. 2, February 1996

The Phase Space of Interactions and the Hebb Rule in the Neural Network Models

Tatsuya UEZU and Kazuo NOKURA*

Department of Physics, Nara Women's University, Nara 630
**Shonan Institute of Technology, Fujisawa 251*

(Received October 4, 1995)

We study the phase space of couplings in neural network models by introducing the overlap with the Hebb rule. Replica calculations and numerical calculations have been performed for both spherical and Ising constraints of the couplings. For small capacity, we find that the Hebb couplings are very close to the Maximally Stable Network (MSN) in both couplings. Further, in the Ising coupling, we study both the replica symmetric and the one-step replica symmetry breaking solutions and discuss which of these solutions is appropriate in several regions in the space of the temperature and the capacity by analyzing numerical results obtained by the enumeration method.

§ 1. Introduction

The study of neural networks has been greatly advanced recently since Gardner[1)] developed the method to treat the problem by statistical mechanics. She introduced the space of interactions and analyzed the volume of interactions by the replica method. Many interesting concepts have been introduced by this approach. Among them, the Maximally Stable Network (MSN) for associative memory has been attracting many authors.

The main aspect of the associative memory is described as follows. Let us consider $N+1$ neurons. The neuron state s_i $(i=0, 1, \cdots, N)$ takes values ± 1. Let J_{ij} be the synaptic coupling strength from a neuron j to i. Then, the time development of s_i is given by

$$s_i(t+1)=\mathrm{sgn}(h_i(\{s(t)\})-\vartheta)\,, \tag{1}$$

where $\mathrm{sgn}(x)=1$ for $x>1$ and -1 for $x\leq 0$, ϑ is a threshold, and $h_i(\{s(t)\})$ is the internal field at time t,

$$h_i(\{s(t)\})=\frac{1}{\sqrt{N}}\sum_{j=1}^{N} J_{ij}s_j(t)\,. \tag{2}$$

A state of neurons, a pattern $\{\xi_0{}^\mu, \xi_1{}^\mu, \cdots, \xi_N{}^\mu\}$, is one of the fixed points of the dynamics (1), provided $\xi_i{}^\mu(h_i(\{\xi^\mu\})-\vartheta)>0$ for all i. Further, to give it a finite basin of attraction, the stronger condition

$$\xi_i{}^\mu(h_i(\{\xi^\mu\})-\vartheta)>\kappa>0 \tag{3}$$

is imposed. The capacity α of a network is defined by the following ratio: the number of patterns which satisfy the condition (3), p, to the number of neurons N, $\alpha=p/N$.

If we assume that J_{ij} is independent of J_{ji}, we can focus on the condition for one neuron, i.e., $i=0$, and study the space $J_j\equiv J_{0j}$. Gardner calculated the typical fractional volume of the space of solutions which satisfy condition (3) for the spherical and the Ising couplings $\{J_j\}$. Here the condition for the spherical coupling is $\sum_{j=1}^{N} J_j^2 = N$, and for the Ising coupling, $J_j = \pm 1$.

On the other hand, the Hopfield model,[2] the spin model with the Hebb coupling $J_{ij} = (1/\sqrt{N})\sum_{\mu=1}^{p}\xi_i^{\mu}\xi_j^{\mu}$, has attracted many researchers, since it allows the analytic evaluation of the thermodynamic properties.[3] The performance of this model is very good for sufficiently small α, but the fixed points of the dynamics become slightly different from $\{\xi_i^{\mu}\}$ for a moderate α, and memory states disappear for $\alpha > 0.14$. This value is much lower than the critical capacity of the MSN, e.g., $\alpha_c = 2.0$ for the spherical coupling. It was shown in Ref. 4) that the MSN trained with noisy patterns is reduced to the Hebb coupling in the large noise limit. Wong et al. discussed the relation between couplings trained with various noise strengths, including the Hebb and the MSN.[5] In their formulation, the type of coupling is controlled by the type of the cost function characterized by the strength of noise. We suppose that the explicit evaluation is worth studying, since the relation between the Hebb and the MSN is an interesting problem.

In this paper, we discuss the relation between the Hebb coupling J_j^0 and the MSN J_j by studying the overlap given by $M = (1/N)\sum_{j=1}^{N} J_j J_j^0$ for the spherical coupling. We derive the asymptotic form for M as $\alpha \to \infty$ and present the corresponding numerical results.

For the Ising coupling, we choose the clipped Hebb coupling for J_j^0, and study M in the framework of not only the replica symmetry (RS) but also the one-step replica symmetry breaking (RSB) proposed in Ref. 6), since the RS solution becomes unstable. In this case, there are three characteristic regions in the space of the temperature and the capacity; i.e., the SS region where only the RS solution exists and is stable, the BS region where the RS solution is stable and the RSB solution exists, and the BU region where the RS solution is unstable and the RSB solution exists. We performed numerical calculations by means of the enumeration method and here discuss the appropriateness of the RS and the RSB solutions. Further, the asymptotic behavior is discussed theoretically and numerically.

In the next section, we formulate the problem and derive the expression of the overlap between the MSN and the Hebb rules. In § 3, we discuss the spherical case, presenting the numerical results. In §§ 4 and 5, the Ising case is discussed, and in § 5 numerical results and their analysis are given in this case. A summary and discussion are given in § 6.

§ 2. Formulation

In this section, we present the general formulation to evaluate the overlap M. We consider the interactions which can memorize all the prescribed p patterns $\{R^{\mu}, \xi_1^{\mu}, \cdots, \xi_N^{\mu}\}$, $\mu = 1 \sim p$, where ξ_i^{μ} takes values ± 1 each with probability 1/2. We put $R^{\mu} \equiv \xi_0^{\mu}$. Further, we impose the condition that the overlap between the concerned interaction $\{J_j\}$ and the other specified rule $\{J_j^0\}$ is fixed to M. M and $\{J_j^0\}$ are expressed as follows:

$$M=\frac{1}{N}\sum_{j=1}^{N}J_jJ_j^0\,,$$

$$J_j^0=f(w_j)\,,$$

$$w_j=\frac{1}{\sqrt{N}}\sum_{\mu=1}^{p}\xi_j^\mu R^\mu\,. \tag{4}$$

We take $f(w)=w$ for the Hebb rule and $f(w)=\mathrm{sgn}(w)$ for the clipped Hebb rule.

For the Ising coupling, the fractional volume of the phase space which satisfies condition (3) is

$$V=\frac{1}{\Omega}\int dM\sum_{\{J_j\}}\Big[\prod_{\mu=1}^{p}\Theta(R^\mu h(\{\xi^\mu\})-\kappa\Big]\delta\Big(M-\frac{1}{N}\sum_j J_jf(w_j)\Big)\,, \tag{5}$$

$$\Omega=2^N\,,$$

where $\sum_{\{J_j\}}$ denotes the summation over all configurations of $\{J_j\}$. The threshold ϑ is put to 0. The function under the integration is the fractional volume of the solutions which have overlap M with the coupling $\{J_j^0\}$. Assuming self-averaging, we take the average of $\ln V$ over the patterns. To achieve this program, we introduce n replicas which have the same realization of p patterns. Further, we introduce the energy and the temperature.[6),7)] The energy for a state $\{J_j\}$ is defined as the number of patterns which cannot be memorized,

$$E[\{J_j\},\xi]=\sum_{\mu=1}^{p}\Theta\Big(\kappa-\frac{R^\mu}{\sqrt{N}}\sum_{j=1}^{N}J_j\xi_j^\mu\Big)\,. \tag{6}$$

The partition function is defined by

$$Z=\int dM\sum_{\{J_j\}}\exp(-\beta E[\{J_j\},\xi])\delta\Big(M-\frac{1}{N}\sum_j J_jf(w_j)\Big)\,, \tag{7}$$

where $\beta=1/T$ is the inverse temperature. As $T\to 0$, Z/Ω tends to V. To calculate $\ln Z$, we use the replica method. The sample average of Z^n can be calculated by introducing other δ functions and using the standard recipe,

$$1=\int\prod_i dw_i\delta\Big(w_i-\frac{1}{\sqrt{N}}\sum_{\mu=1}^{p}\xi_i^\mu R^\mu\Big)$$

$$=\int\prod_i dw_i\frac{d\bar{w}_i}{2\pi}\exp\Big\{i\bar{w}_i\Big(w_i-\frac{1}{\sqrt{N}}\sum_{\mu=1}^{p}\xi_i^\mu R^\mu\Big)\Big\}\,,\quad\text{etc}\,.$$

The results are as follows:

$$\langle Z^n\rangle_\xi=\int d\bar{q}\int d\bar{F}\int d\boldsymbol{M}\int d\bar{\boldsymbol{M}}\int d\boldsymbol{q}_T\int d\bar{\boldsymbol{q}}_T\exp\Big\{NG(\bar{q},\bar{F},\boldsymbol{M},\bar{\boldsymbol{M}},\boldsymbol{q}_T,\bar{\boldsymbol{q}}_T,\beta)\Big\}\,, \tag{8}$$

$$G=i\boldsymbol{M}\bar{\boldsymbol{M}}+i\boldsymbol{q}_T\bar{\boldsymbol{q}}_T-\sum_{\alpha<\beta}F^{\alpha\beta}q^{\alpha\beta}+\alpha G_1(\bar{q},\boldsymbol{q}_T,\beta)+G_2(\bar{F},\bar{\boldsymbol{M}},\bar{\boldsymbol{q}}_T)\,, \tag{9}$$

$$G_1(\bar{q},\boldsymbol{q}_T,\beta)=\ln\Big[\Big\{\prod_a\Big(e^{-\beta}\int_{-\infty}^{\kappa}\frac{d\lambda^a}{2\pi}+\int_{\kappa}^{\infty}\frac{d\lambda^a}{2\pi}\Big)\int dx^a\Big\}$$

$$\times\exp\Bigl(i\sum_\alpha x^\alpha\lambda^\alpha-\frac{1}{2}\sum_\alpha(x^\alpha)^2-\sum_{\alpha<\beta}q^{\alpha\beta}x^\alpha x^\beta-\sum_\alpha q_T{}^\alpha x^\alpha\Bigr)\Bigr],$$

$$G_2(\bar{F},\bar{\boldsymbol{M}},\bar{q}_T)=\ln\Bigl[\sum_{\{J^\alpha\}}\int dw\int\frac{d\bar{w}}{2\pi}$$

$$\times\exp\Bigl\{-i\sum_\alpha\bar{M}^\alpha J^\alpha f(w)+\sum_{\alpha<\beta}F^{\alpha\beta}J^\alpha J^\beta+i\bar{w}w-\frac{\alpha}{2}\bar{w}^2-i\sum_\alpha\bar{q}_T{}^\alpha J^\alpha\bar{w}\Bigr\}\Bigr],$$

$$q^{\alpha\beta}=\frac{1}{N}\sum_i J_i{}^\alpha J_i{}^\beta,$$

where α and β are indices of replicas and $\sum_{\{J\alpha\}}$ denotes the summation over all configurations of $\{J^\alpha\}$. We use abbreviations such as $\bar{q}=\{q^{\alpha\beta}\}$, $\boldsymbol{M}=\{M^\alpha\}$, $d\bar{q}=\prod_{\alpha<\beta}dq^{\alpha\beta}$, $d\boldsymbol{M}=\prod_\alpha dM^\alpha$, etc. In addition to these usual order parameters, we have introduced the order parameter $q_T{}^\alpha=(1/\sqrt{N})\sum_i J_i{}^\alpha w_i$ and its complement $\bar{q}_T{}^\alpha$.

In our calculation, the constraint of $M=(1/N)\sum_{j=1}^N J_j{}^\alpha J_j{}^0$ is imposed on all α. We can obtain the same results in the case that the constraint is imposed on a particular J^α only.

In the next section, we discuss the spherical coupling case.

§ 3. Spherical coupling and Hebb rule

In the following, we study the overlap between the MSN and the Hebb coupling. The function $f(w)$ is set to $f(w)=w$. The summations $\sum_{\{J_i\}}$ in the equations in the previous section are replaced with integrals over J_i with the weight

$$d\mu\{J\}=\delta(\sum_j J_j{}^2-N)\prod_j dJ_j$$

$$=\int\frac{dE}{2\pi}\exp\{iE(\sum_j J_j{}^2-N)\}\prod_j dJ_j\,.$$

With this change, the term iE_α appears in Eq. (9) and $\sum_{\{J^\alpha\}}$ in G_2 is replaced by $\int\exp(i\sum_\alpha E_\alpha(J^\alpha)^2)\prod_\alpha dJ^\alpha$. In this section, we restrict ourselves to the case that $T=0$ and of the replica symmetric solution, because the RS solution is stable as long as α is less than the critical capacity $\alpha_C(\kappa)$ for $T=0$, as shown in Ref. 7). We obtain in the $n\to 0$ limit,

$$\langle\ln V(M)\rangle=\frac{\alpha}{n}G_{1,\mathrm{RS}}+\frac{1}{n}G_{2,\mathrm{RS}}+\frac{E}{2}+\frac{1}{2}qF+iq_T\bar{q}_T+iM\bar{M}\,, \quad (10)$$

$$\frac{1}{n}G_{1,\mathrm{RS}}=\int Dt\ln H(\tilde{X})\,, \quad (11)$$

$$H(X)=\int_X^\infty Dt\,,\quad \tilde{X}=\frac{\kappa+\sqrt{q}\,t+iq_T}{\sqrt{1-q}}\,,\quad Dt=\frac{1}{\sqrt{2\pi}}\exp\Bigl(-\frac{t^2}{2}\Bigr)dt\,,$$

$$\frac{1}{n}G_{2,\mathrm{RS}}=\frac{1}{2}\ln\frac{2\pi}{E+F}+\frac{1}{2(E+F)}\int Dx\int Du\{\sqrt{F}\,u-i\bar{M}f(Y)\}^2\,, \quad (12)$$

$$Y=\frac{1}{\sqrt{F}}(\sqrt{\alpha F-\bar{q}_T{}^2}\,x+\bar{q}_T u)\,.$$

Here we replace E by $(i/2)E$. At the saddle point, all order parameters depend on M. The solution of the saddle point equations are rather complicated, but they are simplified at the M-maximum point of $\langle\ln V(M)\rangle$, where we can set

$$\frac{d\ln V(M)}{dM}=\frac{\partial\ln V(M)}{\partial M}=i\bar{M}=0\,. \tag{13}$$

With this condition and the condition $(\partial/\partial\bar{q}_T)\ln V(M)=0$, we have $q_T=0$. Substituting $\bar{M}=0$ and $q_T=0$ into the saddle point equations, we obtain

$$q=\alpha(1-q)\int Dt\left(\frac{H'(X)}{H(X)}\right)^2, \tag{14}$$

$$M/\sqrt{\alpha}=\sqrt{\alpha}\sqrt{1-q}\int Dt\left(-\frac{H'(X)}{H(X)}\right), \tag{15}$$

where $H'(X)=dH(X)/dX$. The first equation was derived by Gardner. The second equation is the main result of this section. Since $\{J^0\}$ should be normalized to $\sqrt{N}$, we consider $M/|J_i{}^0|=M/\sqrt{\alpha}$. The MSN is achieved in the $q\to1$ limit, which yields

$$1=\alpha\int_{-\kappa}^{\infty}(\kappa+t)^2Dt\,, \tag{16}$$

$$M/\sqrt{\alpha}=\sqrt{\alpha}\int_{-\kappa}^{\infty}(\kappa+t)Dt\,. \tag{17}$$

The κ-dependence of α is given by the first equation. Then M depends on either α or κ only.

Let us consider two limiting cases. When $\kappa\to\infty$, Eqs. (16) and (17) are reduced to $1=\alpha\kappa^2$ and $M=\alpha k$ respectively. Then we have $M/\sqrt{\alpha}=1$. This value implies that the MSN is reduced to the Hebb rule in the $\alpha\to0$ limit. When $\kappa=0$, we obtain $M/\sqrt{\alpha}=1/\sqrt{\pi}\approx0.564$.

The overlap between couplings trained by noisy patterns was studied in Ref. 5). Their result is given by $r_H=\sqrt{\alpha}\langle\Lambda\rangle$. Here $\langle\ \ \rangle$ is the average over the field distribution (FS) of the network. According to Ref. 8), the FS of the MSN is given by $\rho(\Lambda)=\int_{-\infty}^{k}Dx\delta(\Lambda-k)+\Theta(\Lambda-k)\exp(-\Lambda^2/2)/\sqrt{2\pi}$. We can show that, by substituting $\rho(\Lambda)$ into r_H, the MSN case of r_H is identical to $M/\sqrt{\alpha}$ of our result.

We finish this section by presenting our numerical results. In Fig. 1, we depict the α-dependence of $M/\sqrt{\alpha}$ derived from (17) for large κ and the numerical results. The numerical results were obtained using the minimum-overlap algorithm proposed in Ref. 9). The system size N is 60. The number of samples is 200 for all α. The maximum number of learning steps is 100,000, and the learning parameter $c=5.0$. For $\alpha<1.8$, almost all patterns are learned, but for $\alpha\simeq1.8$, about 50 % of the samples fail to learn all patterns with this number of steps. These samples are excluded in the average. Taking into account the smallness of the system size in our numerical calculation, the replica calculation result seems to fit well with the numerical data, except for data with $\alpha\sim1.8$. Rather large error bars result from the small number of samples.

§ 4. Ising coupling and clipped Hebb rule

In this and the next sections, we discuss the Ising coupling case. The function $f(w)$ is set to $f(w)=\mathrm{sgn}(w)$. This section is devoted to studying the RS and the RSB solution of Eq. (9) in the framework of Ref. 6). In the next section, we will give the numerical results obtained by the exact enumeration method and discuss the appropriateness of the RS and the RSB solutions.

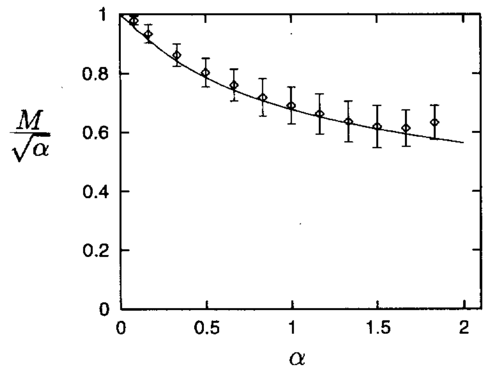

Fig. 1. α-dependence of $M/\sqrt{\alpha}$. Solid curve represents the theoretical result, and diamonds denote numerical data. Error bars are standard deviations over samples.

(a) RS solution

We assume all quantities have replica symmetric properties. Then the RS solution is expressed as follows:

$$\frac{1}{n}G_{\mathrm{RS}}(q, F, M, \bar{M}, q_T, \bar{q}_T, \beta)=i\bar{M}M+\frac{Fq}{2}+i\bar{q}_T q_T$$

$$+\frac{\alpha}{n}G_{1,\mathrm{RS}}(q, q_T, \beta)+\frac{1}{n}G_{2,\mathrm{RS}}(F, \bar{M}, q_T), \tag{18}$$

$$\frac{1}{n}G_{1,\mathrm{RS}}=\int Dt\ln\tilde{H}(\tilde{X}), \quad \tilde{H}(\tilde{X})=e^{-\beta}+(1-e^{-\beta})H(\tilde{X}), \quad \tilde{X}=\frac{\kappa+\sqrt{q}\,t+iq_T}{\sqrt{1-q}},$$

$$\frac{1}{n}G_{2,\mathrm{RS}}=-\frac{F}{2}+\int Dx\int Du\ln[2\cosh\{\sqrt{F}\,u-i\bar{M}f(Y)\}],$$

$$Y=\frac{1}{\sqrt{F}}(\sqrt{\alpha F-\bar{q}_T{}^2}\,x+\bar{q}_T u).$$

As was discussed in § 3, we can impose the conditions $(\partial/\partial M)G_{\mathrm{RS}}=0$ and $(\partial/\partial\bar{q}_T)G_{\mathrm{RS}}=0$ at the M-maximum of G_{RS}. Then we obtain

$$\bar{M}=0, \tag{19}$$

$$q_T=0. \tag{20}$$

Substituting these values into G_{RS}, G_{RS} is reduced to the formula in which there is no constraint on M. The saddle point equations for q, F, $\bar{M}$ and $\bar{q}_T$ are

$$F=\frac{\alpha}{1-q}\int Dt\left(\frac{\tilde{H}'(X)}{\tilde{H}(X)}\right)^2, \tag{21}$$

$$X=\frac{\kappa+\sqrt{q}\,t}{\sqrt{1-q}},$$

$$q=\int Du\tanh^2\sqrt{F}u\ , \tag{22}$$

$$M=\int Dx\int Du\ f(Y)\tanh\sqrt{F}u\ , \tag{23}$$

$$\bar{q}_T=\frac{\alpha}{\sqrt{1-q}}\int Dt\frac{1}{\tilde{H}(X)}|\tilde{H}'(X)|\ . \tag{24}$$

For given parameters α, κ and β, q and F are determined by Eqs. (21) and (22), M is determined by (23) and finally $\bar{q}_T$ is determined by (24). The free energy per synapse f_{RS} and the entropy per synapse S_{RS} are given by

$$f_{RS}(\beta)=\frac{F(1-q)}{2\beta}-\frac{\alpha}{\beta}\int Dt\ln\tilde{H}(X)-\frac{1}{\beta}\int Du\ln[2\cosh\sqrt{F}u]\ , \tag{25}$$

$$S_{RS}=-\frac{F(1-q)}{2}+\alpha\int Dt\ln\tilde{H}(X)$$
$$+\int Du\ln[2\cosh\sqrt{F}u]-\alpha\beta e^{-\beta}\int Dt\frac{H(X)-1}{\tilde{H}(X)}\ . \tag{26}$$

Substituting the solutions q and F into f_{RS} and S_{RS}, f_{RS} and S_{RS} are the functions of α, κ and β. Numerical solutions of these equations appear in Fig. 2 for several values of α (solid curves). As shown in Fig. 2(g), there exist $S<0$ regions.

According to Krauth and Mézard,[6] the transition from RS to RSB is considered to take place when $S_{RS}=0$. Let us define $\alpha_S(\kappa)$ and $T_C(\alpha,\kappa)$ by the following equations.

$$S_{RS}(\alpha_S(\kappa),\ \kappa,\ T=0)=0\ , \tag{27}$$

$$S_{RS}(\alpha,\ \kappa,\ T_C(\alpha,\ \kappa))=0\ . \tag{28}$$

Then, for $\alpha_S(\kappa)<\alpha$ and $T_C(\alpha,\kappa)>T$, $S_{RS}<0$. Thus, the RS solution in this region seems to be inadequate as a solution of the problem. As for the stability of the RS solution, the AT instability takes place at $\alpha\simeq 1.016$ for $\kappa=0$ and $T=0$.[6),10)] Thus before the AT instability takes place, the entropy becomes negative. That is, there are regions of α and T for which the RS solution is stable and the RSB solution exists.

Similar to the spherical case, we investigate the asymptotic behavior as $\kappa\to\infty$. Approximate analytic solutions to Eqs. (21)$\sim$(24) and (27) are obtained:

$$\alpha_s(\kappa)\simeq\frac{2}{\pi\kappa^2}\left[1-\frac{32}{c}\left(\frac{2}{\pi}\right)^{3/2}\frac{(\ln\kappa)^2}{\kappa^4}\right], \tag{29}$$

$$q\simeq 1-\frac{4}{c}\left(\frac{2}{\pi}\right)^{3/2}\frac{\ln\kappa}{\kappa^2}\ , \tag{30}$$

$$F\simeq\frac{\pi^2c^2}{64}\frac{\kappa^4}{(\ln\kappa)^2}\ , \tag{31}$$

$$\bar{q}_T\simeq\frac{c}{4}\sqrt{\frac{\pi}{2}}\frac{\kappa}{\ln\kappa}\ , \tag{32}$$

$$M \simeq 1-\frac{2}{\pi}\frac{1}{\kappa}. \tag{33}$$

See the Appendix for the details. We can see that M tends to 1 as κ increases, that is, the MSN coincides with the clipped Hebb rule for large κ. This is a situation similar to that in the spherical case.

Next, we discuss the RSB solution.

(b) RSB solution

We take the one-step replica symmetry breaking according to Ref. 6), that is,

$$\left.\begin{array}{l} q^{\alpha\beta}=q_0 \\ F^{\alpha\beta}=\hat{q}_0 \end{array}\right\} \text{ for } I\left(\frac{\alpha}{m}\right)\neq I\left(\frac{\beta}{m}\right),$$

$$\left.\begin{array}{l} q^{\alpha\beta}=q_1 \\ F^{\alpha\beta}=\hat{q}_1 \end{array}\right\} \text{ for } I\left(\frac{\alpha}{m}\right)=I\left(\frac{\beta}{m}\right) \text{ and } \alpha\neq\beta,$$

where $I(x)$ is an integer valued function: its value is the smallest integer greater than or equal to x. For other quantities, the replica symmetry is assumed. Following Krauth and Mézard, we derive the one-step RSB solution:

$$\begin{aligned}
&\frac{1}{n}G_{\mathrm{RSB}}(q_0, \hat{q}_0, q_1, \hat{q}_1, M, \bar{M}, q_T, \bar{q}_T, \beta, m) \\
&\quad = i\bar{M}M+\frac{1}{2}[mq_0\hat{q}_0+(1-m)q_1\hat{q}_1]+i\bar{q}_T q_T \\
&\qquad +\frac{\alpha}{n}G_{1,\mathrm{RSB}}(q_0, q_1, q_T, \beta, m)+\frac{1}{n}G_{2,\mathrm{RSB}}(\hat{q}_0, \hat{q}_1, \bar{M}, \bar{q}_T, m), \\
&\frac{1}{n}G_{1,\mathrm{RSB}}=\frac{1}{m}\int Dz_0 \ln\left\{\int Dz_1 \tilde{H}(\bar{X})^m\right\}, \\
&\bar{X}=\frac{\kappa+\sqrt{q_0}z_0+\sqrt{q_1-q_0}\,z_1+iq_T}{\sqrt{1-q_1}}, \\
&\frac{1}{n}G_{2,\mathrm{RSB}}=-\frac{\hat{q}_1}{2}+\frac{1}{m}\int Dx\int Du \ln\left\{\int Dz_1 (2\cosh W)^m\right\}, \\
&W=\sqrt{\hat{q}_0}\,u+z_1\sqrt{\hat{q}_1-\hat{q}_0}-i\bar{M}f(Y), \quad Y=\frac{1}{\sqrt{\hat{q}_0}}(\sqrt{\alpha\hat{q}_0-\bar{q}_T{}^2}\,x+\bar{q}_T u).
\end{aligned} \tag{34}$$

If we impose the conditions $(\partial/\partial M)G_{\mathrm{RSB}}=0$ and $(\partial/\partial\bar{q}_T)G_{\mathrm{RSB}}=0$, then $\bar{M}=0$ and $q_T=0$ follow. Substituting these values into Eq. (34), G_{RSB} reduces to the function without constraint on M, which agrees with that derived by Krauth and Mézard. They stated in their paper[6)] that the results of their numerical calculation strongly suggest that there exist solutions only when $q_1\to 1$ and $\hat{q}_1\to\infty$. Thus, we take this limit in the expression G_{RSB} of Eq. (34). Then,

$$\frac{1}{n}G_{1,\mathrm{RSB}}(q_0, 1, q_T, \beta, m)=\frac{1}{m}\int Dz_0 \ln\left\{e^{-\beta m}+(1-e^{-\beta m})H\left(\frac{\kappa+\sqrt{q_0}z_0+iq_T}{\sqrt{1-q_0}}\right)\right\}, \tag{35}$$

$$\frac{1}{n}G_{2,\mathrm{RSB}}(\hat{q}_0, \infty, \bar{M}, \bar{q}_T, m)$$

$$=\frac{m}{2}(\hat{q}_1-\hat{q}_0)-\frac{\hat{q}_1}{2}+\frac{1}{m}\int Dx\int Du\ \ln[2\cosh m\{\sqrt{\hat{q}_0}u-i\bar{M}f(Y)\}]\,. \tag{36}$$

Therefore,

$$\frac{1}{n}G_{\mathrm{RSB}}(q_0, \hat{q}_0, 1, \infty, M, \bar{M}, q_T, \bar{q}_T, \beta, m)$$

$$=-\frac{m}{2}\hat{q}_0(1-q_0)+i\bar{M}M+i\bar{q}_Tq_T+\frac{1}{m}\int Dx\int Du\ln[2\cosh m\{\sqrt{\hat{q}_0}u-i\bar{M}f(Y)\}]$$

$$+\frac{\alpha}{m}\int Dz_0\ln\left\{e^{-\beta m}+(1-e^{-\beta m})H\left(\frac{\kappa+\sqrt{q_0}z_0+iq_T}{\sqrt{1-q_0}}\right)\right\}. \tag{37}$$

From these equations, we obtain

$$G_{\mathrm{RSB}}(q_0, \hat{q}_0, 1, \infty, M, \bar{M}, q_T, \bar{q}_T, \beta, m)$$

$$=\frac{1}{m}G_{\mathrm{RS}}(q_0, m^2\hat{q}_0, M, m\bar{M}, q_T, m\bar{q}_T, \beta m)\,. \tag{38}$$

The saddle point equations for the RSB solution are

$$\hat{q}_0=\left(\frac{\beta}{\beta_C}\right)^2F_C\,, \tag{39}$$

$$q_0=q_C\,, \tag{40}$$

$$M=M_C\,, \tag{41}$$

$$\bar{q}_T=\frac{\beta}{\beta_C}\bar{q}_{T,C}\,, \tag{42}$$

$$m=\frac{\beta_C}{\beta}\,, \tag{43}$$

where F_C, q_C and β_C are determined by the saddle point equations for the RS solution and the condition $S_{\mathrm{RS}}(q_C, F_C, \beta_C)=0$. M_C and $\bar{q}_{T,C}$ are M and $\bar{q}_T$ for the RS solution at $\beta=\beta_C$. That is, q_0 and M are constant. The free energy and the entropy are also constant:

$$f_{\mathrm{RSB}}(\beta)=f_{\mathrm{RS}}(\beta=\beta_C)=\text{constant}\,, \tag{44}$$

$$S_{\mathrm{RSB}}(\beta)=S_{\mathrm{RS}}(\beta=\beta_C)=0\,. \tag{45}$$

The overlap function becomes

$$P(q)=\frac{T}{T_C}\delta(q-q_C)+\left(1-\frac{T}{T_C}\right)\delta(q-1)\,. \tag{46}$$

Thus, we obtain the mean value of the overlap $q^{\alpha\beta}$,

$$q_{av} \equiv \int dq P(q) q = \frac{T}{T_C} q_C + 1 - \frac{T}{T_C}, \tag{47}$$

which increases from q_C to 1 as T decreases from T_C to 0.

In Fig. 2, the temperature dependence of M, q_{av}, S and f are depicted for several values of α (dashed curves).

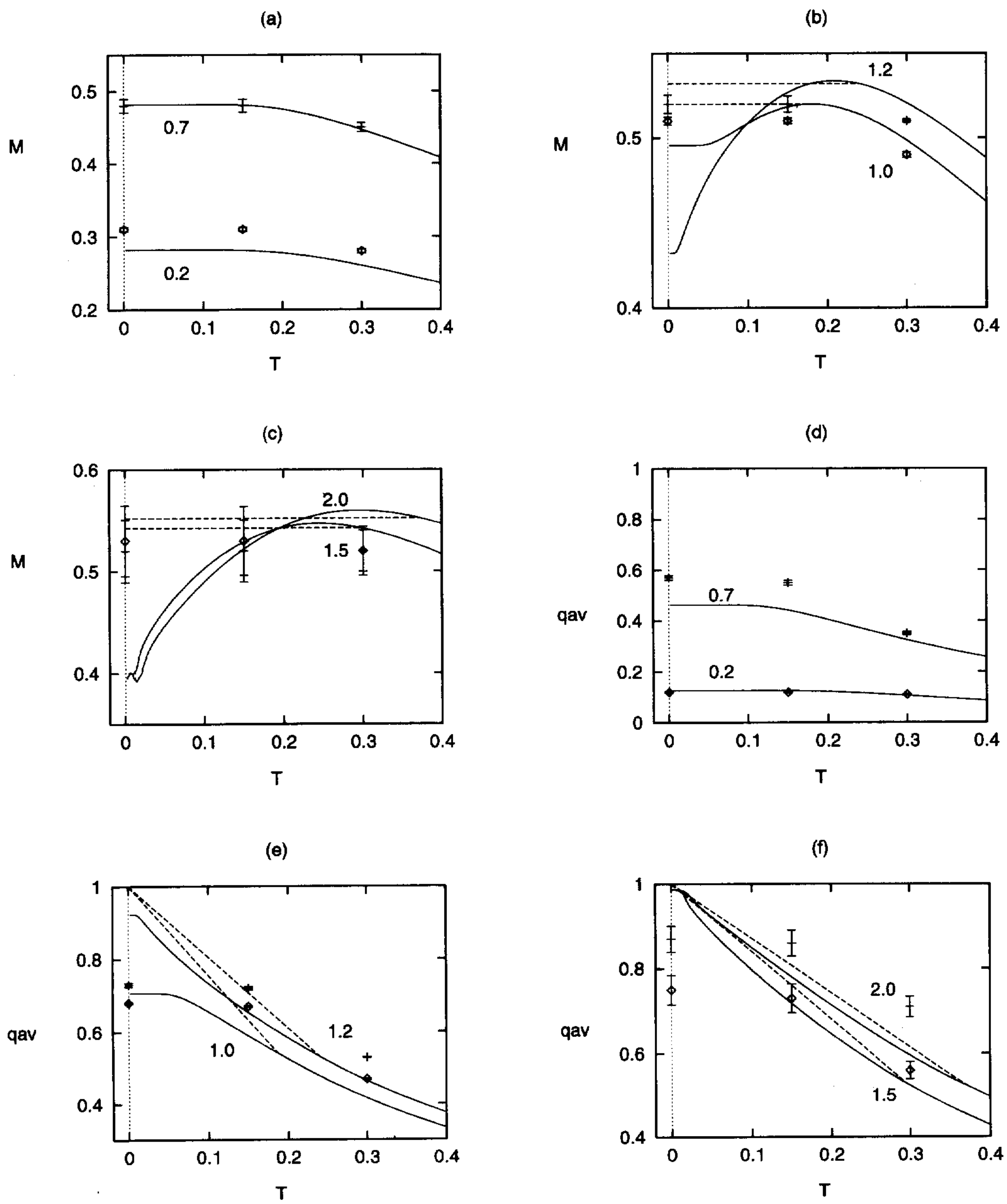

Fig. 2. (continued)

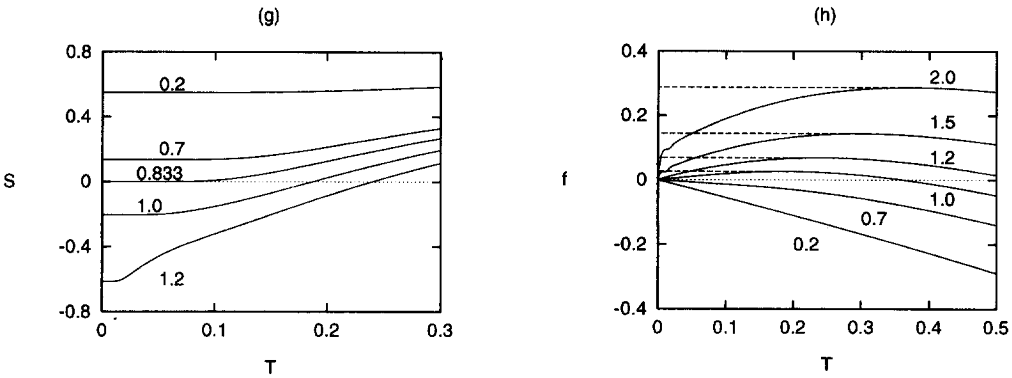

Fig. 2. Temperature dependence of M, q_{av}, entropy S_{RS} and free energy f. κ is fixed to 0. Solid curves and dashed curves denote the RS solutions and the RSB solutions, respectively. ◇ and + denote numerical results. Error bars are also depicted with them.

(a) M. ◇ : α=0,2, + : α=0.7.
(b) M. ◇ : α=1.0, + : α=1.2, $T_C \simeq 0.1868(\alpha=1.0)$, $0.2397(\alpha=1.2)$.
(c) M. ◇ : α=1.5, + : α=2.0, $T_c \simeq 0.2970(\alpha=1.5)$, $0.3724(\alpha=2.0)$.
(d) q_{av}. ◇: α=0.2, + : α=0.7.
(e) q_{av}. ◇: α=1.0, + : α=1.2, $T_C \simeq 0.1868(\alpha=1.0)$, $0.2397(\alpha=1.2)$.
(f) q_{av}. ◇: α=1.5, + : α=2.0, $T_C \simeq 0.2970(\alpha=1.5)$, $0.3724(\alpha=2.0)$.
(g) Entropy S_{RS} for various α.
(h) Free energy f for various α.

(c) Existence and stability of solutions.

As mentioned above, the RSB solution appears for $\alpha > \alpha_S(\kappa)$ and $T < T_C(\kappa, \alpha)$. On the other hand, the boundary of the stability of the RS solution is determined by Eqs. (21), (22) and the following equations:

$$\frac{1}{(1-q)^2}\int Dt\left(\frac{\tilde{H}'(X)}{\tilde{H}(X)}\right)^2\left\{X+\frac{\tilde{H}'(X)}{\tilde{H}(X)}\right\}^2\int Dt\frac{1}{\cosh^4(\sqrt{F}\,t)}=1\,. \tag{48}$$

These equations determine the critical value of α, $\alpha_{AT}(\kappa, T)$. For $\alpha > \alpha_{AT}(\kappa, T)$, the RS solution is unstable. In Fig. 3, the stability and the existence diagram of the solutions is shown for $\kappa=0$. There are the following three regions in the diagram:

SS: only the RS solution exists and is stable.

BS: the RS solution is stable and the RSB solution exists.

BU: the RS solution is unstable and the RSB solution exists.

As for the free energy per synapse f, the RSB free energy is greater than the RS free energy when both solutions exist. See Fig. 2(h).

In the next section, we present the method and the results of numerical calculations to check our theoretical results.

§ 5. Numerical calculation

Now, we present numerical calculations to study the behavior of q_{av} and M. We first summarize the theoretical results in which we are interested, and then describe the numerical method and give the numerical results.

According to the replica study, the (T, α) space is divided into three regions, BU, BS and SS, and the expressions for M and q_{av} are different for the RS and the RSB solutions, as discussed in § 4. M and $q_{av}=q$ for the RS solution are given by Eqs. (22) and (23), which change nonlinearly as T is decreased to 0. On the other hand, in the RSB solution given by Eqs. (39)~(47), M is constant and q_{av} increases linearly up to 1 as T is decreased to 0. Their behavior is depicted in Figs. 2(a)~(f).

We are also interested in the situation where M tends to 1. This is achieved by taking the limit $\kappa\to\infty$ at $\alpha=\alpha_s(\kappa)$, and then M is given by Eq. (33).

Now, we describe the numerical method.

In our calculation, the system size N was taken from 5 to 15, and we enumerated all configurations of synapse states, 2^N states for each sample.

The thermodynamic average and the sample average are taken as follows. Let α be one of the synapse states for a given set of patterns $\{\xi^\mu\}$. The thermodynamic average of a quantity A is defined as $\langle A\rangle=\sum_\alpha P_\alpha A_\alpha$, where A_α is the value in the synapse state α and $P_\alpha=e^{-\beta E_\alpha}/\sum_\alpha e^{-\beta E_\alpha}$ and E_α is the energy of the state α. In the case $T=0$, only ground states were taken into account in the above summation. In the finite temperature case, in the summation we included such states that their energies are less than some fixed value which depends on the temperature. That is, we took synapse states with energies up to E_0+1 and E_0+2 for $T=0.15$ and for $T=0.3$, respectively. Here, E_0 is the minimum energy. The sample average is defined by $\overline{\langle A\rangle}=(1/N_S)\sum_\xi\langle A\rangle$, where N_S is the number of samples. We checked that the upper bounds of energies and the number of samples we took were sufficient to ensure the accuracy of the second digit for M and q_{av}, at least for $N\leq 15$. That is, the addition of the next energy states to the summation in the thermodynamic average cause a change only in the third digit of the average values. As for the numbers of samples, we increased the number of samples until the average values fluctuated at the third digit.

Next, we present our numerical results on the behavior of the overlap with the Hebb rule M and the average overlap q_{av} for $\kappa=0$.

We treated six values of α, $\alpha=0.2$, 0.7, 1.0, 1.2, 1.5 and 2.0, and three cases of the temperature, $T=0$, 0.15 and 0.3. These values of α and T are located in the three regions as follows:

SS; $\alpha=0{,}2$ and all T, $\alpha=0.7$ and all T, $\alpha=1.0$ and $T=0.3$, $\alpha=1.2$ and $T=0.3$, $\alpha=1.5$ and $T=0.3$.

BS; $\alpha=1.0$ and $T=0$, $\alpha=1.0$ and $T=0.15$, $\alpha=1.2$ and $T=0.15$, $\alpha=2.0$ and $T=0.3$.

BU; $\alpha=1.2$ and $T=0$, $\alpha=1.5$ and $T=0$, 0.15, $\alpha=2.0$ and $T=0$, 0.15.

See Fig. 3 and the Table.

We took the following values of p/N for each α.

$$\alpha\simeq 2.0\ :\ \frac{p}{N}=\frac{21}{11},\ \frac{25}{13},\ \frac{29}{15},$$

$$\alpha\simeq 1.5\ :\ \frac{p}{N}=\frac{17}{11},\ \frac{19}{13},\ \frac{23}{15},$$

$$\alpha\simeq 1.2\ :\ \frac{p}{N}=\frac{7}{5},\ \frac{9}{7},\ \frac{11}{9},\ \frac{13}{11},\ \frac{15}{13},\ \frac{17}{15},$$

$$\alpha=1\quad :\ N=p=5,\ 7,\ 9,\ 11,\ 13,\ 15,$$

$$\alpha\simeq 0.7\ :\ \frac{p}{N}=\frac{3}{5},\ \frac{5}{7},\ \frac{7}{9},\ \frac{7}{11},\ \frac{9}{13},\ \frac{11}{15},$$

$$\alpha\simeq 0.2\ :\ \frac{p}{N}=\frac{1}{5},\ \frac{1}{7},\ \frac{3}{9},\ \frac{3}{11},\ \frac{3}{13},\ \frac{3}{15}.$$

The sample average depends on N and p, $\overline{\langle A(N, p/N)\rangle}$. For each α, the above values of p/N are different from α. To obtain the average $\overline{\langle A(N,\alpha)\rangle}$ from the average $\overline{\langle A(N, p/N)\rangle}$, we made a linear extrapolation about α. For example, to obtain $\overline{\langle A(N, \alpha=1.2)\rangle}$, we made a linear extrapolation using data for $\alpha\simeq 1.2$ and $\alpha=1$. The same procedure was performed for other values of α. Next, for a fixed α, to obtain the $N=\infty$ limit from the values of $\overline{\langle A(N,\alpha)\rangle}$, we made the extrapolation about N. That is, assuming the dependence on N of the average $\overline{\langle A(N,\alpha)\rangle}$ as $\overline{\langle A(N,\alpha)\rangle}=A^*+\tilde{A}/N$, we determined A^* and $\tilde{A}$ by the method of the least squares.

For later use, we define the relative deviation of a quantity A^* as follows:

$$r_A\equiv|(A_{\text{th}}-A^*)/A^*|\times 100(\%),$$

where A_{th} is the theoretical value of $\overline{\langle A(N=\infty,\alpha)\rangle}$.

In Fig. 4, $\overline{\langle M(N,\alpha)\rangle}$ v.s. $1/N$ and $q_{av}(N,\alpha)=\overline{\langle q(N,\alpha)\rangle}$ v.s. $1/N$ plots are shown for several parameters. Numerical results for the $N=\infty$ limits are listed in the Table together with the values of r. In the Table, deviations in A^* and $\tilde{A}$ from the $1/N$ fitting, which are denoted by δA^* and $\delta\tilde{A}$, are also listed. Also in Figs. 2(a)~(f), A^* and δA^* are shown with theoretical results.

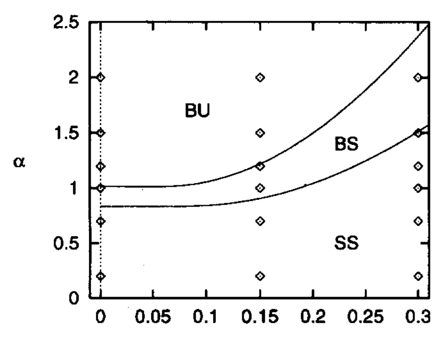

Fig. 3. Temperature dependence of $\alpha_S(\kappa=0, T)$ (lower curve) and $\alpha_{AT}(\kappa=0, T)$ (upper curve). These curves separate (T,α) space into three regions, SS, BS and BU. Diamonds denote the points at which numerical calculations are performed.

General tendency

Several examples of $\overline{\langle M(N,\alpha)\rangle}$ v.s. $1/N$ and $\overline{\langle q(N,\alpha)\rangle}$ v.s. $1/N$ plots are displayed in Fig. 4. From these, we note that there exist scatterings of data around fitting lines. This suggests the possibility of a nonlinear fitting of data.

A similar situation occurred in a study of the capacity.[11] However, as the deviations from the $1/N$ fitting, δA^* and $\delta\tilde{A}$, are rather small, as shown in the Table, we only considered the $1/N$ fitting of the data. As for the temperature dependence, the values for $T=0$ and 0.15 are similar, but those for $T=0.3$ differ from these for almost all data. See the Table. The temperature dependence becomes weaker as α becomes smaller. We think that this is because there are many low energy states for small α, and the effect of the temperature is less significant.

Overlap with the clipped Hebb rule M

BU region

In this region, the RS solution is unstable. The extrapolated values M^* to $N=\infty$ from numerical data are close to the values of the RSB solutions and $r_M^{(\mathrm{RSB})}=2\sim6\ \%$.

BS region

The RS and the RSB values are nearly equal in this region. Both $r_M^{(\mathrm{RS})}$ and $r_M^{(\mathrm{RSB})}$ range from $1\ \%\sim3\ \%$.

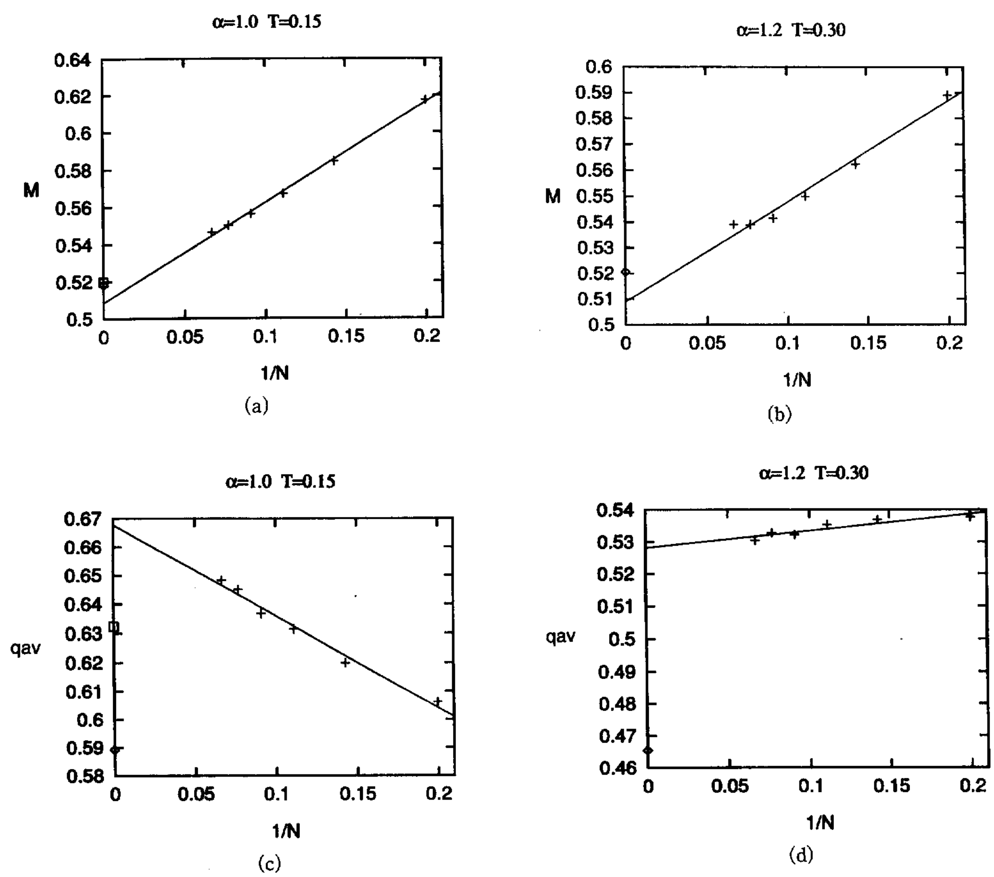

Fig. 4. $1/N$ fitting for $\overline{\langle M(N,\alpha)\rangle}$ and $\overline{\langle q(N,\alpha)\rangle}$. (a), (b): $\overline{\langle M(N,\alpha)\rangle}$ v.s. $1/N$, (c), (d): $\overline{\langle q(N,\alpha)\rangle}$ v. s. $1/N$. (a), (c): $\alpha=1.0$, $T=0.15$, (b), (d): $\alpha=1.2$, $T=0.3$. Symbols + denote numerical data. A diamond and a square denote the RS solution and the RSB solution, respectively. The fitting lines are obtained by the method of the least squares.

Table. List of $A^{(RS)}$, $A^{(RSB)}$, the extrapolated values to $N=\infty$ A^* and the gradient $\tilde{A}$ for M and q_{av} together with values of r for each α and T. The errors δM^*, $\delta\tilde{M}$, δq^* and $\delta\tilde{q}$ and the regions for each values of α and T are also shown.

(a) M, (b) q_{av}.

(a) M

α	T	$M^{(RS)}$	$M^{(RSB)}$	M^*	δM^*	$\tilde{M}$	$\delta\tilde{M}$	$r_M^{(RS)}$	$r_M^{(RSB)}$	region
0.2	0.0	0.282	—	0.31	0.016	0.34	0.13	8.3	—	SS
	0.15	0.281	—	0.31	0.016	0.34	0.13	8.2	—	SS
	0.3	0.260	—	0.28	0.012	0.35	0.097	6.9	—	SS
0.7	0.0	0.481	—	0.48	0.0021	0.55	0.017	0.60	—	SS
	0.15	0.481	—	0.48	0.0021	0.55	0.017	0.94	—	SS
	0.3	0.447	—	0.45	0.0022	0.44	0.018	0.37	—	SS
1.0	0.0	0.496	0.520	0.51	0.0013	0.54	0.010	2.7	2.0	BS
	0.15	0.518	0.520	0.51	0.0012	0.54	0.0093	1.9	2.2	BS
	0.3	0.499	—	0.49	0.0018	0.42	0.015	1.8	—	SS
1.2	0.0	0.449	0.532	0.52	0.0024	0.51	0.020	14	1.7	BU
	0.15	0.527	0.532	0.52	0.0025	0.50	0.02	0.80	1.8	BS
	0.3	0.521	—	0.51	0.0024	0.39	0.019	2.3	—	SS
1.5	0.0	0.423	0.543	0.53	0.016	0.54	0.198	20	2.0	BU
	0.15	0.529	0.543	0.53	0.015	0.54	0.195	0.2	2.4	BU
	0.3	0.542	—	0.52	0.008	0.44	0.105	4.2	—	SS
2.0	0.0	0.422	0.552	0.52	0.006	0.72	0.079	19	6.2	BU
	0.15	0.522	0.552	0.52	0.006	0.71	0.079	0.38	6.2	BU
	0.3	0.560	0.552	0.52	0.005	0.55	0.065	7.7	6.2	BS

(b) q_{av}

α	T	$q_{av}^{(RS)}$	$q_{av}^{(RSB)}$	q_{av}^*	δq_{av}^*	$\tilde{q}_{av}$	$\delta\tilde{q}_{av}$	$r_q^{(RS)}$	$r_q^{(RSB)}$	region
0.2	0.0	0.127	—	0.12	0.0030	0.090	0.024	2.0	—	SS
	0.15	0.126	—	0.12	0.0027	0.083	0.022	0.94	—	SS
	0.3	0.106	—	0.11	0.0030	0.052	0.024	5.0	—	SS
0.7	0.0	0.463	—	0.57	0.0093	−0.36	0.076	19	—	SS
	0.15	0.442	—	0.55	0.0090	−0.27	0.073	20	—	SS
	0.3	0.324	—	0.35	0.0064	0.21	0.052	8.7	—	SS
1.0	0.0	0.706	1	0.68	0.0024	−0.38	0.020	3.3	46	BS
	0.15	0.589	0.632	0.67	0.0017	−0.32	0.014	12	5.3	BS
	0.3	0.417	—	0.47	0.0016	0.16	0.013	11	—	SS
1.2	0.0	0.892	1	0.73	0.0055	−0.45	0.045	22	37	BU
	0.15	0.654	0.708	0.72	0.0048	−0.40	0.039	9.0	1.5	BS
	0.3	0.465	—	0.53	0.0010	0.053	0.0078	12	—	SS

(continued)

	0.0	0.956	1	0.75	0.035	−0.30	0.44	14	33	BU
1.5	0.15	0.718	0.761	0.73	0.034	−0.24	0.43	1.6	4.2	BU
	0.3	0.524	—	0.56	0.020	0.30	0.26	6.4	—	SS
	0.0	0.956	1	0.87	0.031	−1.22	0.39	9.9	15	BU
2.0	0.15	0.780	0.807	0.86	0.030	−1.19	0.39	9.3	6.1	BU
	0.3	0.595	0.615	0.71	0.024	−0.71	0.31	16	13	BS

SS region

Except for $\alpha=0.2$, $r_M{}^{(\mathrm{RS})}$ is 0.5 %$\sim$4 % and for $\alpha=0.2$, $r_M{}^{(\mathrm{RS})}\sim 8$ %.

The values of the RSB solution in the BU region and those of the RS solution in the SS region agree with numerical results. However, in the BS region, since the numerical result is between the RS and the RSB solutions, we cannot determine which is more consistent with the numerical results. We think this is because the RS and the RSB solutions are similar in this region.

The mean value of the overlap $q^{\alpha\beta}$, q_{av}

BU region

For $T=0$, the RSB value must be 1. q^* is about 0.73 for $\alpha=1.2$, 0.75 for $\alpha=1.5$, and 0.87 for $\alpha=2.0$. $r_q{}^{(\mathrm{RSB})}$ ranges from 15$\sim$40 %. For $T\neq 0$, $r_q{}^{(\mathrm{RSB})}=4\sim 16$ %.

BS region

In this region, for $\alpha=2.0$, $T=0.3$, for $\alpha=1.2$, $T=0.15$ and for $\alpha=1$, $T=0.15$, the RSB is most consistent with the numerical results. But for $\alpha=1$, $T=0$, the RS is most consistent. The values of $r_q{}^{(\mathrm{RS})}$ and $r_q{}^{(\mathrm{RSB})}$ fluctuate largely.

SS region

In this region, $r_q{}^{(\mathrm{RS})}=1$ %$\sim$20 %.

As is seen from Figs. 2(e) and (f), q_{av} increases when T decreases or α increases. This behavior is in accordance with the theory.

From the above results, we note two points on the precision. Contrary to the case of M, the values of $r_q{}^{(\mathrm{RS})}$ are large. The agreement between theoretical results and numerical values is not good, even in the region SS. The values $r_q{}^{(\mathrm{RS})}$ are about 1$\sim$20 % in this region, contrary to the case M, $r_M{}^{(\mathrm{RS})}=0.5\sim 8$ %. Since the results for M in the SS region are consistent with the theoretical results, the RS ansatz seems to be appropriate in this region. Thus, in the q_{av} case, the value of r_q of order 1$\sim$20 % is considered to be a consistent result in our calculation.

Another point is about the $T=0$ calculations. In the BU region, $r_q{}^{(\mathrm{RSB})}=15\sim 40$ % and $r_q{}^{(\mathrm{RS})}=10\sim 22$ %. Since these values are too large compared with other data, our calculations of q_{av} for $T=0$ do not seem sufficient.

Taking into account the above consideration and putting the results for M and q_{av} cases together, we conclude that theoretical values of the RSB solutions in the BU region and those of the RS solutions in the SS region are consistent with our numerical results. However, we cannot conclude whether the RS or the RSB solution is more consistent in the BS region.

Finally, the asymptotic behavior of the solution as $\kappa \to \infty$ is investigated.

We set $T=0$. To observe the asymptotic tendency, calculations for $\kappa=1.8$ and $p/N=3/15$, and for $\kappa=0$ and $p/N=15/15$ are performed. The theoretical predictions for $\kappa=0$ are $\alpha_S \simeq 0.833$ and $M=0.499$. For $\kappa=1.8$, $\alpha_S=0.136$ and $M=0.700$. Our numerical result for $\kappa=0$ and $p/N=15/15$ is $M=0.548(0.126)$. For $\kappa=1.8$ and $p/N=3/15$, $M=0.607(0.170)$. Values in the parentheses are standard deviations over samples. Numerical results are consistent with theoretical predictions, showing increasing tendency as κ increases.

§ 6. Summary and discussion

In this paper, we considered the phase space of interactions in neural network models and studied the nature of the synaptic couplings introducing the overlap M with the Hebb rule or the clipped Hebb rule. We treated both the spherical coupling and the Ising coupling by the replica method.

As is shown in Ref. 8), in the spherical coupling, the RS solution is stable as long as α is less than the critical capacity. The situation is a little complicated for the Ising coupling. In this case, the critical capacity $\alpha_S(\kappa)$ is determined by the equation $S_{RS}=0$. For $\alpha_S(\kappa)<\alpha$ and $T_C>T$, the RSB solution appears. $\alpha_S(\kappa=0)\sim 0.833$ and the AT instability of the RS solution takes place at $\alpha_{AT}(\kappa=0, T=0)\simeq 1.016$. That is, there are regions of α and T in which the RS solution is stable and the RSB solution exists (the BS region). We investigated the appropriateness of the RS and the RSB solutions.

We calculated M and the mean overlap q_{av} both theoretically and numerically. For M, the theoretical estimate is about 0.5 for small κ in both couplings. This implies that the synaptic couplings which memorize the given p patterns are similar to the Hebb or the clipped Hebb coupling. Further, we found theoretically that M increases to 1 as κ increases for both types of the couplings.

To check the behavior of M for large κ for the spherical case, the numerical calculation was made, and fairly good agreement between the theoretical and the numerical results was obtained.

For the Ising coupling, we investigated three cases, the SS (only the RS solution exists and is stable), the BS (the RS solution is stable and the RSB solution exists) and the BU (the RS solution is unstable and the RSB solution exists) cases. We performed numerical calculations and evaluated M and q_{av} to check the theoretical results. It appears that the convergence in the calculation of M is very good, but that of q_{av} is not so good. From our results, it seems that further calculation is required to obtain the large N limit behavior for q_{av} in the BS and the BU regions, especially in $T=0$ case. We discuss this further below.

Putting numerical results in M and q_{av} together, we conclude that theoretical predictions are consistent with numerical results. That is, the RS solution in the SS region and the RSB solution in the BU region are most consistent. However, in the BS region, we could not determine which of the RS or the RSB solution is more consistent with numerical data, because the convergence is not good, and/or the difference between the RS and the RSB values is small in both theoretical and numerical results.

The asymptotic behavior for $\kappa \gg 1$ (equivalently for $\alpha \ll 1$) was also investigated numerically, and consistent results were obtained. The numerical results show the increasing tendency of M as κ increases, as the theory predicts.

Since our numerical calculation treats a finite number of neurons, we took into account finite size effects to obtain the result for $N=\infty$. We made a linear fitting of the data in terms of $1/N$ and obtained fairly good results. We adopted the enumeration method to generate all configurations of N neurons and made sample averages. The precision of our results is two digits, that is, the third digit fluctuates. We think that our results are exact up to the number of neurons $N=15$ since we made the enumeration. So, it is meaningful to look at more details of our numerical results. From our numerical results, we note the following. Although δM^* and $\delta\tilde{M}$ are nearly constant for all temperatures, δq^* and $\delta\tilde{q}$ increase as T is lowered. And δq^* and $\delta\tilde{q}$ are much greater than δM^* and $\delta\tilde{M}$. For example, for $T=0$, δq^* and $\delta\tilde{q}$ are nearly two times greater than δM^* and $\delta\tilde{M}$. That is, the characteristic feature in our numerical calculation is that the values of r_q are greater than those of r_{M}. The precision in the calculation of q_{av} is not good. Let us take an example. At $\alpha=1.0$ and $T=0$, the BS region, the theoretical value of q_{av} is 1 for the RSB and 0.71 for the RS, but the numerical values are 0.68, that is $r_q^{(\mathrm{RS})}\simeq 3\,\%$ and $r_q^{(\mathrm{RSB})}\simeq 46\,\%$. On the other hand, $r_M^{(\mathrm{RS})}\simeq r_M^{(\mathrm{RSB})}\simeq 2\,\%$ with the same parameter values. Though the RS solution would seem to be more appropriate in the former case, considering other results for different parameters, it is not conclusive that the RS solution is appropriate in this region.

For large values of α or for small values of N and p, there are few solutions satisfying condition (3), and the total number of solutions is too small to represent the large N characteristics of solutions. By our enumeration method, we could take the number of neurons up to $N=15$. To obtain a sufficient number of low energy states for the calculation of q_{av} and to obtain conclusive results in the case of BS, it is necessary to perform numerical calculations for a larger number of neurons using other methods. This approach is left as a future problem.

Acknowledgements

We would like to thank Mrs. Miki Usui and Miss Naomi Nakamura for their assistance in the numerical calculations.

Appendix
— *Asymptotic Solution* —

In this Appendix, we calculate the asymptotic solutions to Eqs. (21)~(24) and (27) for $\kappa \gg 1$.

Using the asymptotic form of $H(X)\simeq \exp(-X^2/2)/\sqrt{2\pi}X$ for $X\gg 1$, we obtain from Eq. (21),

$$F\simeq \frac{\alpha\kappa^2}{(1-q)^2}+\frac{\alpha}{1-q}\,. \tag{1}$$

As suggested by this equation, we assume $F \gg 1$, and then Eq. (22) is

$$1-q \simeq \frac{1}{\sqrt{F}}\left(\sqrt{\frac{2}{\pi}}-\frac{c}{F}\right), \tag{2}$$

where $c=(1/\sqrt{2\pi})\sum_{n=0}^{\infty}(-1)^{n-1}/n^2=\pi^2/12\sqrt{2\pi}$. Substituting Eq. (2) into Eq. (1), we obtain

$$F \simeq \alpha\kappa^2 F\left(\frac{\pi}{2}+2\left(\frac{\pi}{2}\right)^{3/2}\frac{c}{F}\right)+\sqrt{F}\,\alpha\sqrt{\frac{\pi}{2}}. \tag{3}$$

The term of $O(1)$ cannot be neglected to get a consistent result. Equation (3) is rewritten as

$$F\left(1-\frac{\pi}{2}u^2\right) \simeq \alpha\sqrt{\frac{\pi}{2}}\sqrt{F}+2\left(\frac{\pi}{2}\right)^{3/2}cu^2, \tag{4}$$

$$u^2 \equiv \alpha\kappa^2. \tag{5}$$

As the right-hand side of Eq. (4) is positive, the condition for α is

$$0<\alpha<\frac{2}{\pi}\frac{1}{\kappa^2}, \tag{6}$$

thus

$$\varepsilon^2 \equiv \sqrt{\frac{2}{\pi}}-u>0. \tag{7}$$

Then the entropy S_{RS} becomes

$$S_{\mathrm{RS}} \simeq \frac{\alpha}{2}\left(1+\frac{\pi}{2}c\frac{u^2}{\alpha\sqrt{F}}+\ln\frac{1-q}{\kappa^2}\right). \tag{8}$$

$\alpha_S(\kappa)$ is determined by the equation $S_{\mathrm{RS}}=0$. Thus, $u^2/\alpha\sqrt{F}$ must be large for $\kappa \gg 1$. Then, from Eq. (4), we obtain

$$F \simeq \frac{c}{\varepsilon^2}\frac{\left(1-\sqrt{\frac{\pi}{2}}\varepsilon^2\right)^2}{1-\frac{1}{2}\sqrt{\frac{\pi}{2}}\varepsilon^2}. \tag{9}$$

From this equation, $\varepsilon \ll 1$ follows because $F \gg 1$, and thus

$$F \simeq \frac{c}{\varepsilon^2}, \tag{10}$$

$$q \simeq 1-\sqrt{\frac{2}{\pi}}\frac{1}{\sqrt{F}} \simeq 1-\sqrt{\frac{2}{\pi}}\frac{\varepsilon}{\sqrt{c}}. \tag{11}$$

Thus, the equation $S_{\mathrm{RS}}=0$ is reduced to

$$\sqrt{c}\frac{\varepsilon}{\alpha}\simeq\ln\frac{1}{\varepsilon\alpha}. \tag{12}$$

From this equation, we obtain

$$\varepsilon\simeq-\frac{2}{\sqrt{c}}\alpha\ln\alpha. \tag{13}$$

Therefore, the following asymptotic expressions of the solutions are derived:

$$\alpha_S(\kappa)\simeq\frac{2}{\pi\kappa^2}\left[1-\frac{32}{c}\left(\frac{2}{\pi}\right)^{3/2}\frac{(\ln\kappa)^2}{\kappa^4}\right], \tag{14}$$

$$\varepsilon^2\simeq\frac{64}{\pi^2 c}\frac{(\ln\kappa)^2}{\kappa^4}, \tag{15}$$

$$q\simeq 1-\frac{4}{c}\left(\frac{2}{\pi}\right)^{3/2}\frac{\ln\kappa}{\kappa^2}, \tag{16}$$

$$F\simeq\frac{\pi^2c^2}{64}\frac{\kappa^4}{(\ln\kappa)^2}. \tag{17}$$

The asymptotic form of $\bar{q}_T$ is obtained to be

$$\bar{q}_T\simeq\frac{\alpha\kappa}{1-q}\simeq\frac{c}{4}\sqrt{\frac{\pi}{2}}\frac{\kappa}{\ln\kappa}. \tag{18}$$

The precise expression of the overlap with the Hebb rule M is

$$M=2\int_0^\infty Du\left\{1-2H\left(\frac{\delta}{\gamma}u\right)\right\}\tanh(\sqrt{F}u), \tag{19}$$

$$\gamma=\frac{\sqrt{\alpha F-\bar{q}_T{}^2}}{\sqrt{F}},$$

$$\delta=\frac{\bar{q}_T}{\sqrt{F}}.$$

Since $\delta/\gamma\simeq\kappa\gg 1$, M becomes

$$M\simeq 1-4\int_0^\infty DuH(\kappa u),$$

$$\simeq 1-\frac{2}{\pi}\frac{1}{\kappa}. \tag{20}$$

References

1) E. Gardner, J. of Phys. **A21** (1988), 257.
2) J. J. Hopfield, Proc. Nat. Acad. Sci. U.S.A. **79** (1982), 2554.
3) D. J. Amit, H. Gutfreund and H. Sompolinsky, Ann. of Phys. **173** (1987), 30.
4) K. Y. M. Wong and D. Sherrington, J. of Phys. **A23** (1990), L175.
5) K. Y. M. Wong, A. Rau and D. Sherrington, Europhys. Lett. **19** (1992), 559.
6) W. Krauth and M. Mézard, J. de Phys. **50** (1989), 3057.
7) E. Gardner and B. Derrida, J. of Phys. **A21** (1988), 271.

8) E. Gardner, J. of Phys. **A22** (1989), 1969.
9) W. Krauth and M. Mézard, J. of Phys. **A20** (1987), L745.
10) W. Krauth and M. Opper, J. of Phys. **A22** (1989), L519.
11) B. Derrida, R. B. Griffiths and A. P-Bennett, J. of Phys. **A24** (1991), 4907.